# Effect of Si doping and applied pressure upon magnetostructural properties of $Tb_5(Si_xGe_{1-x})_4$ magnetocaloric compounds

Yuan-Chieh Tseng,[1,*] Hao-Jhong Ma,[1] Chao-Yao Yang,[1] Yaroslav Mudryk,[2] Vitalij K. Pecharsky,[2,3]
Karl A. Gschneidner Jr.,[2,3] Narcizo M. Souza-Neto,[4] and Daniel Haskel[4]

[1]*Department of Materials Science and Engineering, National Chiao Tung University, Hsin-chu 30010, Taiwan*
[2]*Division of Materials Science and Engineering, The Ames Laboratory, Ames, Iowa 50011-3020, USA.*
[3]*Department of Materials Science and Engineering, Iowa State University, Ames, Iowa 50011-2300, USA.*
[4]*Advanced Photon Source, Argonne National Laboratory, Argonne, Illinois 60439, USA*

The composition- and pressure-dependent magnetostructural properties of $Tb_5(Si_xGe_{1-x})_4$ ($x = 0.4$, 0.485, 0.625, and 0.7) were investigated using x-ray powder diffraction and x-ray magnetic circular dichroism in a diamond anvil cell, respectively. Substituting the smaller-size Si for Ge stabilizes a single-phase, ferromagnetic (FM) orthorhombic O(I) structure for $x \geqslant 0.7$. Similarly, application of external pressure causes a canted antiferromagnetic orthorhombic O(II) sample ($x = 0.4$) to transform into an FM O(I) phase at 4 GPa. The element- and orbital-specific x-ray absorption data indicate that the Tb $4f$ orbital occupation changes with external pressure, likely through $4f$-$5d$ electronic mixing, yet no changes in Tb $4f$ electronic structure are observed with Si doping. The results point to different mechanisms behind the enhancement of FM exchange interactions in $Tb_5(Si_xGe_{1-x})_4$ with chemical and applied pressure, respectively.

## I. INTRODUCTION

In recent years, magnetic refrigeration technology has been considered an alternative to traditional vapor-compression refrigeration because of its environmentally friendly nature.[1–3] Materials exhibiting a strong magnetocaloric effect[4] (MCE) are at the heart of magnetic cooling technology. Among numerous magnetocaloric material candidates, the $R_5(Si_xGe_{1-x})_4$ family ($R$ = rare earth) has drawn much attention due to the strong coupling between structural and magnetic properties that leads to a giant MCE.[3,5–8] The best-known members of the family, $Gd_5(Si_xGe_{1-x})_4$ compounds,[2,3] show a linearly increasing Curie temperature ($T_C$) with Si doping up to near room temperature, greatly enhancing the potential of magnetic cooling for room temperature applications. Replacing Gd with Tb modifies the magnetic properties significantly[9–11] partly due to the different single-ion anisotropies (Gd is isotropic while the $4f$ electron wave functions of Tb lack spherical symmetry) and modifications in the electronic band structure. Key differences between $Gd_5(Si_xGe_{1-x})_4$ and $Tb_5(Si_xGe_{1-x})_4$ include the persistence of antiferromagnetism (AFM) to much higher Si concentrations in the Tb case and the decoupling of magnetic and structural transitions for $0.35 < x < 0.65$ in the Tb family[9] versus the coupled magnetostructural transition for $x \leqslant 0.5$ in the Gd family.[2,3]

The magnetostructural properties of $Tb_5(Si_xGe_{1-x})_4$ are less studied relative to its $Gd_5(Si_xGe_{1-x})_4$ counterpart. Our previous studies have focused on the Si-Ge sites of $Gd_5(Si_xGe_{1-x})_4$, understanding the correlation between bond-breaking and magnetic ordering during the first-order, coupled magnetostructural transitions,[3,12] as well as the correspondence between Si doping (chemical pressure) and applied pressure in enhancing the magnetic ordering temperature, using x-ray magnetic circular dichroism (XMCD) at low temperature and high pressures.[13–15] This work is aimed at understanding the influence of the rare-earth site on the magnetostructural

phase diagram, probing the nature of the uncoupled magnetic and structural transitions for $Tb_5(Si_xGe_{1-x})_4$ and their evolution with Si doping and pressure. We present results from x-ray diffraction experiments showing that the four chosen samples ($x = 0.4$, 0.485, 0.625, and 0.7) are characterized by different structural ground states. These, in turn, are intimately connected to the compounds' magnetic properties and their response to applied pressure, as probed by XMCD measurements. The complexity of the $Tb_5(Si_xGe_{1-x})_4$ system contrasts with that of $Gd_5(Si_xGe_{1-x})_4$, where a ferromagnetic orthorhombic (I) [FM O(I)] ground state is observed for $x \geqslant 0.125$. This work facilitates the understanding of the interplay between magnetism, electronic structure, and crystal structure in the $Tb_5(Si_xGe_{1-x})_4$ system .

## II. EXPERIMENT

Polycrystalline powder samples of $Tb_5(Si_xGe_{1-x})_4$ with $x = 0.4$, 0.485, 0.625, and 0.7 were prepared as described by Zou *et al.*[16] These four compositions were chosen because they cover the region of the $Tb_5(Si_xGe_{1-x})_4$ phase diagram where magnetic and structural transitions decouple by 5–10 K.[9] This allows a direct comparison with $Gd_5(Si_xGe_{1-x})_4$ which displays a fully coupled magnetostructural transition for $x \leqslant 0.5$. The samples were ground into fine powders for x-ray measurements. Low-temperature (10 K) powder x-ray diffraction (XRD) measurements were performed at the BL01C2 beamline of the National Synchrotron Radiation Research Center (NSRRC), Taiwan, with a wavelength of 0.495941 Å (25 keV). Two-dimensional diffraction patterns were collected by a Mar345 image plate, and the collected diffraction rings were integrated with the FIT2D program[17] into a diffraction pattern of intensity versus scattering angle $2\theta$. Rietveld refinement[18] was used to determine the crystallographic structures and the lattice constants. The low-temperature crystal structures of $x = 0.485$ and 0.625

samples were verified independently using data obtained from a standard rotating-anode powder diffractometer equipped with a low-temperature attachment and Mo $K\alpha$ radiation.[19] The magnetization studies [isothermal and isofield field-cooled (FC), and zero-field-cooled (ZFC) measurements] were conducted using a superconducting quantum interference device (SQUID) magnetometer. The high-pressure (HP) x-ray magnetic circular dichroism setup[13] located at beamline 4-ID-D of the Advanced Photon Source at Argonne National Laboratory was employed to probe the pressure-induced magnetic transitions of the samples. The gap between the pole pieces of an electromagnet needed to accommodate the diamond anvil cell[13] resulted in a magnetic field ($H$) of ~0.45 T. The XMCD signals were collected over the Tb $L_3$ edge ($2p \rightarrow 5d$ electric dipole transition at 7.514 keV) in helicity-switching mode, and data accuracy was verified by consecutive measurements under reverse applied field. X-ray absorption near-edge structure (XANES) spectra were simultaneously acquired to monitor changes in the electronic structure with Si doping and applied pressure.

## III. RESULTS

The XRD patterns measured at 10 K and ambient pressure condition for the four samples, together with Rietveld refinements using the models of monoclinic (M), orthorhombic (I) [O(I)], orthorhombic (II) [O(II)], and mixed-phase [M + O(I)], are presented in Fig. 1. The results reveal the ground-state crystal structures of the samples. The $Tb_5(Si_{0.4}Ge_{0.6})_4$ compound is characterized by a single-phase, O(II) structure. Both $Tb_5(Si_{0.485}Ge_{0.515})_4$ and $Tb_5(Si_{0.625}Ge_{0.375})_4$ are mixed-phase M + O(I) compounds, with $Tb_5(Si_{0.625}Ge_{0.375})_4$ having a larger volume fraction of the O(I) phase than $Tb_5(Si_{0.485}Ge_{0.515})_4$. The $Tb_5(Si_{0.7}Ge_{0.3})_4$ compound presents a single-phase, O(I) structure. The concentrations of the M phase were ~53% (65%) and ~15% (25%) for $Tb_5(Si_{0.485}Ge_{0.515})_4$ and $Tb_5(Si_{0.625}Ge_{0.375})_4$, respectively, based on the data recorded using rotating-anode (synchrotron) radiation. The variation in absolute phase fractions for each composition may be attributed to different preferred orientations of physically different specimens used in the two types of measurements.

Figure 2 shows the *M-H* curves for the four samples at $T = 10$ K, the same temperature at which the XRD patterns were collected. The inset shows the saturation magnetization ($M_s$) and remnant magnetization ($M_r$) as a function of Si content and O(I) concentration. The $Tb_5(Si_{0.4}Ge_{0.6})_4$ sample exhibits a hysteresis loop that is far from square, and magnetization that only approaches saturation at ~4 T. The significant hysteresis accompanying the change in field direction, as indicated by the arrows, suggests a possible partially irreversible field-induced AFM $\rightarrow$ FM phase transition, similar to the observation in $Gd_5Ge_4$.[20,21] Alternatively, the presence of competing AFM and FM interactions in zero field could be responsible for the reduced (but finite) $M_r$ and observed differences in FC and ZFC data [Fig. 3(a)]. For the other three samples, the concentration of the ferromagnetic component (as derived from the squareness of the hysteresis loop, remanence, and low-field saturation) increases with Si doping; all samples show much reduced hysteresis compared to $Tb_5(Si_{0.4}Ge_{0.6})_4$.
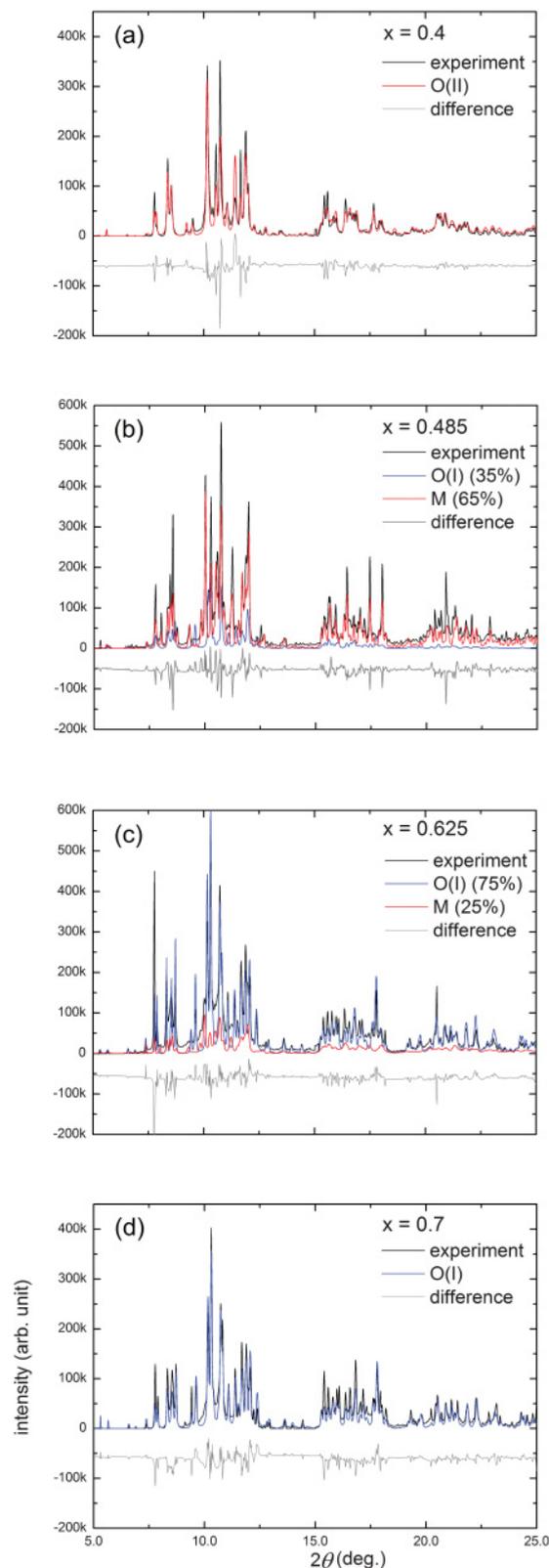


FIG. 1. (Color online) X-ray diffraction patterns of (a) $Tb_5(Si_{0.4}Ge_{0.6})_4$, (b) $Tb_5(Si_{0.485}Ge_{0.515})_4$, (c) $Tb_5(Si_{0.625}Ge_{0.375})_4$, and (d) $Tb_5(Si_{0.7}Ge_{0.3})_4$ at $T = 10$ K, together with results of Rietveld refinements using models of single-phase O(II) (a), mixed-phase M + O(I) (b) and (c), and single-phase O(I) (d) crystal structures. Gray lines at the bottom of the plot represent the difference between the experimental and theoretical intensities.
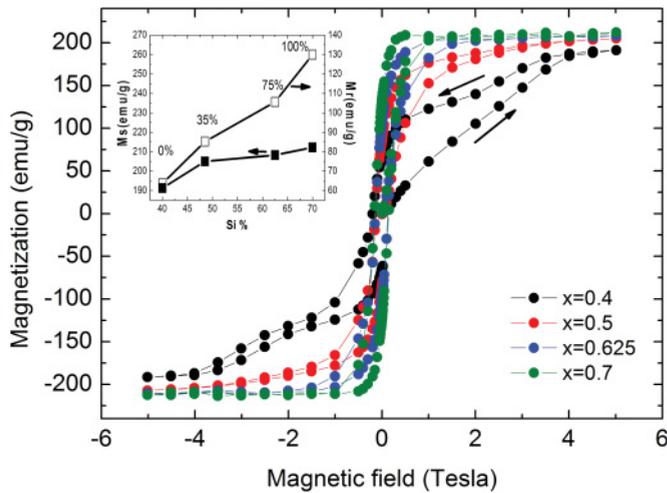
FIG. 2. (Color online) Isothermal *M-H* data for $Tb_5(Si_{0.4}Ge_{0.6})_4$, $Tb_5(Si_{0.485}Ge_{0.515})_4$, $Tb_5(Si_{0.625}Ge_{0.375})_4$, and $Tb_5(Si_{0.7}Ge_{0.3})_4$, collected at $T = 10$ K. Arrows indicate the directions of the change of magnetic field in $Tb_5(Si_{0.4}Ge_{0.6})_4$. The inset shows $M_s$ (filled squares, left-hand axis) and $M_r$ (open squares, right-hand axis) as a function of Si content. The O(I) concentrations for the four samples are marked on top of the open squares.

The samples reach a saturation magnetization of $\sim 200$ emu/g at 5 T, the value reported by Zou *et al.*[22] in a single-crystal $Tb_5(Si_{0.55}Ge_{0.45})_4$ sample with the magnetic field applied along the **a** axis (the easy magnetization direction). Since the saturation magnetization is markedly different for field applied along the **b** and **c** directions, our data indicate that the powder samples were oriented in the field (easy axis along the field direction). The slightly reduced saturation for $x = 0.4$ is likely due to an incomplete field-induced AFM[O(II)] $\rightarrow$ FM[O(I)] transition in this sample. These trends in *M-H* curves for $Tb_5(Si_{0.485}Ge_{0.515})_4$, $Tb_5(Si_{0.625}Ge_{0.375})_4$, and $Tb_5(Si_{0.7}Ge_{0.3})_4$ correlate well with the increasing fraction of the O(I) phase detected from XRD, which is generally linked to a FM phase in the $R_5(Si_xGe_{1-x})_4$ family (see inset in Fig. 2). In addition, these data are consistent with previous reports[11,16] showing that the saturation magnetization of the monoclinic phase is smaller than that of the O(I) phase.

Temperature-dependent FC and ZFC measurements on warming are summarized in Fig. 3, showing the magnetic properties of the four samples and their evolution with Si doping. An increase in transition temperature from 70 to 210 K is observed with increasing Si content, consistent with the magnetostructural phase diagram.[7] Nevertheless, a notable irreversibility between FC and ZFC data is observed in $Tb_5(Si_{0.4}Ge_{0.6})_4$, $Tb_5(Si_{0.485}Ge_{0.515})_4$, and $Tb_5(Si_{0.625}Ge_{0.375})_4$ samples; the irreversibility diminishes with increasing Si concentration and finally nearly disappears in $Tb_5(Si_{0.7}Ge_{0.3})_4$.

Temperature-dependent integrated XMCD intensities for $Tb_5(Si_{0.4}Ge_{0.6})_4$ at various pressures are shown in Fig. 4(a). The nonzero XMCD at ambient pressure and low temperature is due to either the canting of an AFM structure under the $H = 0.45$ T applied field or the presence of reduced ferromagnetism due to competing AFM and FM interactions in the $x = 0.4$ sample. Irreversibility in FC and ZFC SQUID
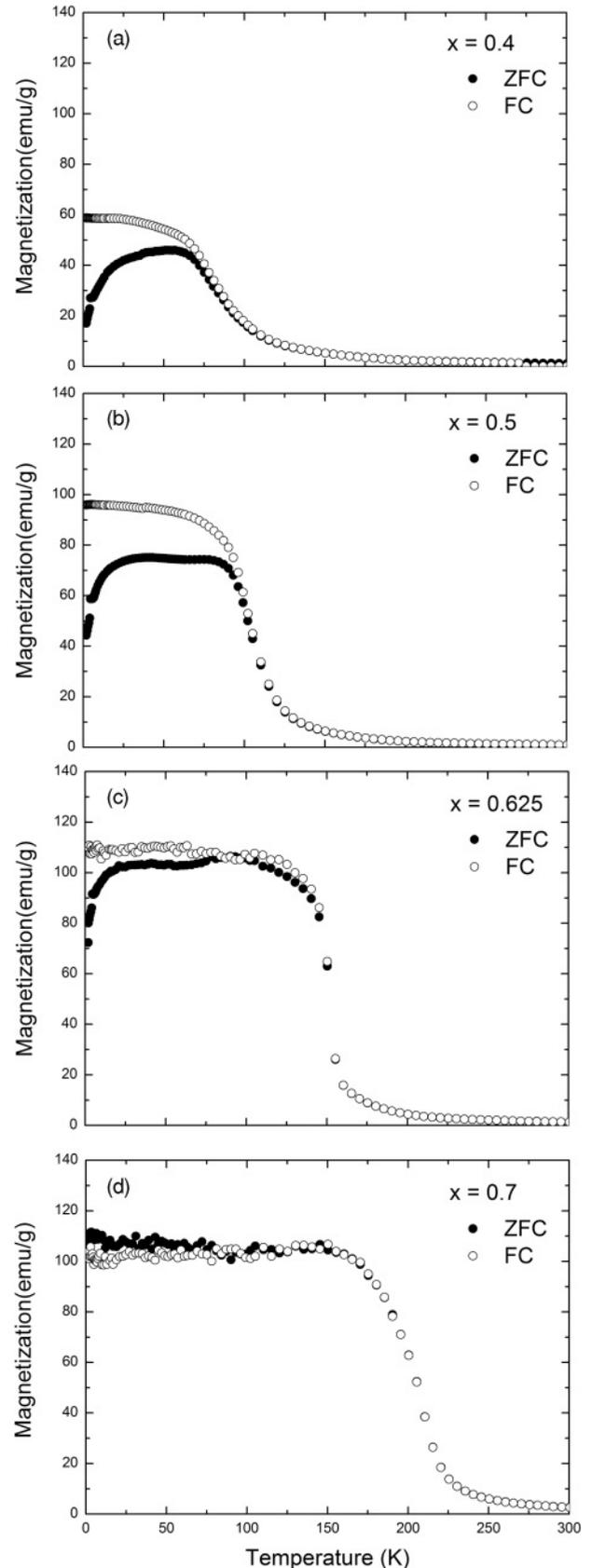


FIG. 3. Temperature-dependent magnetization data of (a) $Tb_5(Si_{0.4}Ge_{0.6})_4$, (b) $Tb_5(Si_{0.485}Ge_{0.515})_4$, (c) $Tb_5(Si_{0.625}Ge_{0.375})_4$, and (d) $Tb_5(Si_{0.7}Ge_{0.3})_4$ measured on warming at $H = 0.45$ T, after field cooling (open circles) and zero-field cooling (filled circles).
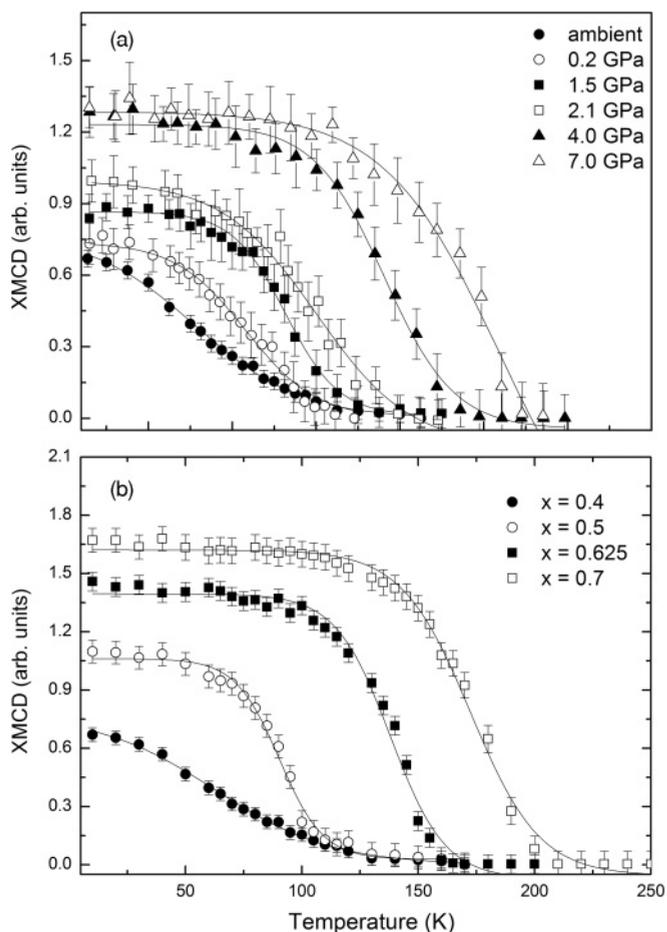
FIG. 4. Temperature-dependent integrated XMCD data of (a) $Tb_5(Si_{0.4}Ge_{0.6})_4$ taken at various pressures and (b) $Tb_5(Si_{0.4}Ge_{0.6})_4$, $Tb_5(Si_{0.485}Ge_{0.515})_4$, $Tb_5(Si_{0.625}Ge_{0.375})_4$, and $Tb_5(Si_{0.7}Ge_{0.3})_4$ taken at ambient pressure. Both data sets were measured on warming. The lines are guides to the eye.
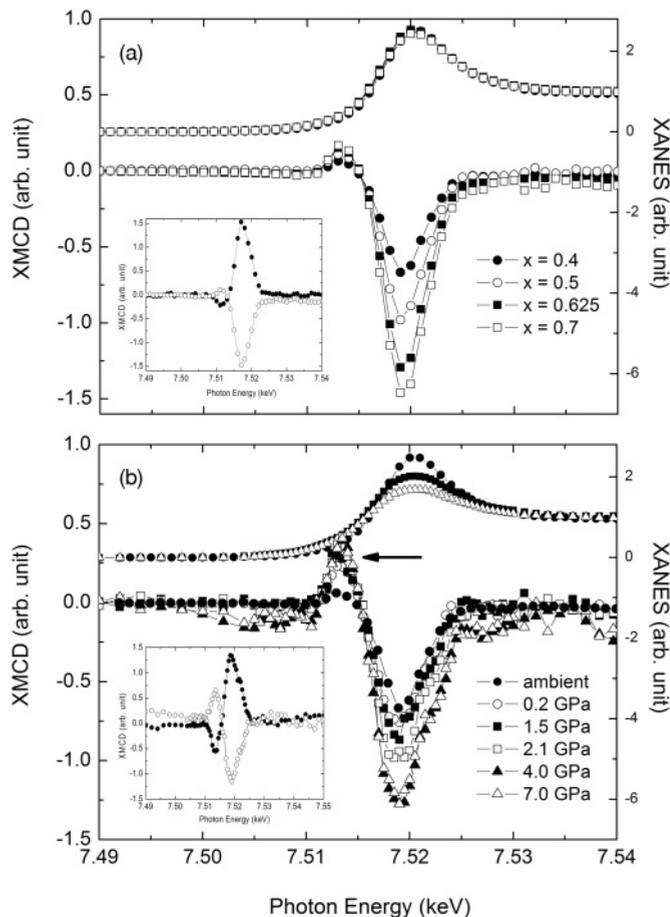


FIG. 5. (a) Doping- and (b) pressure-dependent ($x = 0.4$) Tb $L_3$-edge XANES (upper curves) and XMCD (lower curves) data. Arrows indicate the numeral scales for XANES (right axis) and XMCD (left axis). The XMCD data are normalized to the absorption jump. Data were collected at $H = 0.45$ T and $T = 10(2)$ K. The insets show the reversal of XMCD signal upon reversal of the applied field. For clarity, XANES data in (b) are only shown at ambient pressure and 1.5 and 7.0 GPa.

data (Fig. 3), together with finite remnant magnetization (Fig. 2), indicate that the latter scenario is more likely. The enhanced XMCD signals at higher pressures are due to a pressure-induced stabilization of the FM state. The details will be discussed below. Figure 4(b) shows temperature-dependent, integrated XMCD intensities at ambient condition for the four samples. Figures 4(a) and 4(b) depict the correspondence between pressure and Si doping in affecting the magnetic properties.

Figure 5 presents the (a) Si- and (b) pressure-dependent Tb $L_3$-edge XMCD data collected at $T = 10(2)$ K (normalized to the x-ray absorption jump). XANES spectra for both are also displayed to show where the XMCD quadrupolar ($2p \rightarrow 4f$) and dipolar signals are located relative to the edge. The insets confirm the reversal of the XMCD signal upon field switching. The data reveal the details for the electronic modifications upon Si doping and increasing pressure. As expected, the magnetization is enhanced by both Si doping and applied pressure, which is consistent with what has been found in the low-$x$, mixed-phase regime ($x \leqslant 0.125$) of $Gd_5(Si_xGe_{1-x})_4$.[13] For the pressure-dependent result, the XMCD signal does not increase any further in the $4-7$ GPa range, indicating that a fully saturated FM state has been reached. Although

the XMCD signal at base temperature reaches saturation, the magnetic ordering temperature keeps increasing from 4 to 7 GPa as shown in Fig. 4(a).

For the $L_3$-edge XMCD of rare-earth compounds, it is expected that the quadrupolar ($2p \rightarrow 4f$) and dipolar ($2p \rightarrow 5d$) contributions dominate the onset and higher excitation energies of the spectrum, respectively.[23–25] For the pressure-induced transition [Fig. 5(b)], the XMCD quadrupolar contribution becomes more prominent with the increase of pressure, whereas it is barely noticeable with Si doping [Fig. 5(a)]. The enhancement of the quadrupolar channel occurs along with an asymmetric broadening of the XMCD line shape and a decrease in XANES white line peak intensity. Although the decrease in XANES peak intensity could be due to band broadening alone, the concomitant increase in the $4f$ contribution is likely indicative of a change in orbital occupation. The different responses of the XMCD quadrupolar contribution to doping and pressure can be clearly seen in the inset panels of Figs. 5(a) and 5(b), which correspond to the
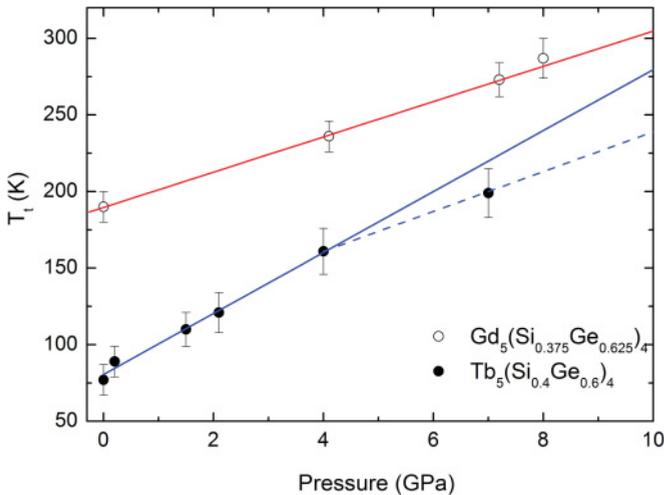
FIG. 6. (Color online) Pressure dependencies of $T_t$ for $Gd_5(Si_{0.375}Ge_{0.625})_4$ (open circles, taken from Ref. 23) and $Tb_5(Si_{0.4}Ge_{0.6})_4$ (filled circles). Dashed line shown for $Tb_5(Si_{0.4}Ge_{0.6})_4$ corresponds to a $dT_t/dP$ of ~1.35 K kbar$^1$ for $P > 4$ GPa, which is close to 1.5 K kbar$^{-1}$ observed in $Gd_5(Si_{0.375}Ge_{0.625})_4$. Solid line for $Tb_5(Si_{0.4}Ge_{0.6})_4$ is the extrapolation of the low-pressure linear behavior.

largest chemical ($x = 0.7$) and physical pressure ($P = 7$ GPa), respectively.

Figure 6 compares the pressure dependence of magnetic transition temperature, $dT_t/dP$, for $Gd_5(Si_{0.375}Ge_{0.625})_4$ and $Tb_5(Si_{0.4}Ge_{0.6})_4$, where the data for $Gd_5(Si_{0.375}Ge_{0.625})_4$ are taken from our previous work.[26] The pressure dependence of $T_t$ for $Tb_5(Si_{0.4}Ge_{0.6})_4$ is obtained from Fig. 4(a), in which $T_t$ is defined as the maximum in the absolute value of the data's first derivative. Generally, this $T_t$ corresponds to a 60% reduction in XMCD signal relative to its saturated value at low $T$. These two particular compounds were chosen because of their close Si content, allowing us to compare $dT_t/dP$ in the different structural ground states of the two families [$Gd_5(Si_{0.375}Ge_{0.625})_4$ is O(I), but $Tb_5(Si_{0.4}Ge_{0.6})_4$ is O(II) at ambient pressure]. As can be seen in the figure, $Tb_5(Si_{0.4}Ge_{0.6})_4$ exhibits a larger $dT_t/dP$ (1.9 K kbar$^{-1}$) than $Gd_5(Si_{0.375}Ge_{0.625})_4$ (1.5 K kbar$^{-1}$) up to 4 GPa. However, the two become comparable after $P = 4$ GPa.

## IV. DISCUSSION

As follows from the $M(H)$ and $M(T)$ data shown in Figs. 2 and 3, the O(II) structure of $Tb_5(Si_{0.4}Ge_{0.6})_4$ results in a canted AFM O(II) (weakly ferromagnetic) magnetostructural ground state in zero field. This is expected since at this Si doping level ferromagnetic interactions only begin to compete with predominantly AFM interactions. This is in fair agreement with the magnetostructural phase diagram of $Tb_5(Si_xGe_{1-x})_4$ reported by Ritter et al.,[7] in which the AFM O(II) ground state is present up to $x \sim 0.35$. The presence of magnetocrystalline anisotropy,[9,10] together with the polycrystalline nature of the sample, results in nonzero FM signal in magnetization data. The $R_5(Si_xGe_{1-x})_4$ compounds are quite sensitive to applied field, temperature, and pressure, all of which affect the interslab bonding. As a consequence, the significant hysteresis

seen in the $M(H)$ data of $Tb_5(Si_{0.4}Ge_{0.6})_4$ is likely due to a field-induced canted AFM $\rightarrow$ FM transition, similar to what is observed in $Gd_5Ge_4$.[20,21] The transition is complete at $\mu_0 H = 4$ T, and the magnetization as a function of the reduced field refers to the remaining FM fraction as a result of hysteresis. The influence of the applied field on the canted AFM O(II) phase of $Tb_5(Si_{0.4}Ge_{0.6})_5$ may also be responsible for a significant irreversibility between ZFC and FC data on warming.

A mixed [M + O(I)] ferromagnetic state for $Tb_5(Si_{0.5}Ge_{0.5})_4$ has been reported by Morellon et al.,[11,27] where both M and O(I) structures are found to support long-range FM ordering. However, the ferromagnetic [M + O(I)] ground state reported here for $Tb_5(Si_{0.485}Ge_{0.515})_4$ and $Tb_5(Si_{0.625}Ge_{0.375})_4$ samples (determined by XRD and SQUID data) is not fully consistent with the previous findings.[11,27] In our study, the monoclinic phase is observed even at temperatures as low as 10 K, while Morellon et al.[11] report 100% O(I) phase already at $T = 85$ K for $Tb_5Si_2Ge_2$. Such discrepancy may originate from the fact that our samples have slightly different Si : Ge ratios when compared to $Tb_5Si_2Ge_2$, especially considering that properties of alloys in the $Tb_5(Si_xGe_{1-x})_4$ system are quite sensitive to the variation of composition ($x$). However, we believe that the main difference in the phase content at low temperatures originates from the difference in the chemical purity of the rare-earth metals used in the preparation of the alloys. In our study we have used the most pure Tb prepared by Materials Preparation Center (MPC) of Ames Laboratory, which has significantly lower amounts of interstitial impurities (oxygen, nitrogen, and carbon) compared to the commercially available metals used in Ref. 9. In a closely related $Gd_5Si_xGe_{4-x}$ system, the lower purity of the starting Gd metal promotes the formation of the O(I) phase. For example, Hardy et al.[28] report a significant concentration ($\sim$30%) of FM component in the zero-field-cooled $M(H)$ data for the $Gd_5Ge_4$ compound, which is not found in the high-purity $Gd_5Ge_4$ sample.[29] Since the O(II) $Gd_5Ge_4$ structure does not support ferromagnetism, it is a clear indication that the impurities promote formation of the O(I) FM structure in the $Gd_5(Si_xGe_{1-x})_4$ system. Another characteristic example of the purity effect on the magnetostructural behavior in $R_5T_4$ ($T$ is $(Si_xGe_{1-x})$) systems is the $Er_5Si_4$ compound. The structural O(I) to M transition was observed upon cooling in this system in the samples that were prepared using high-purity erbium,[30,31] but the sample prepared using the commercially available Er contains the O(I) phase only at all measured temperatures.[32] Therefore, it is reasonable to assume that using lower-purity Tb (as in Ref. 9) promotes the stability of the O(I) phase in the $Tb_5Si_xGe_{4-x}$ series of alloys, while our samples prepared using high-purity Tb may and do indeed contain measurable amounts of the monoclinic phase.

In general, the O(I) structure describes a slab-connected, fully ordered FM state. Thus, the FM-M state can be thought of as a suppressed FM state due to the magnetic frustration arising from the partially disconnected slabs of the M structure. The magnetic moment of the Tb atoms located closer to the broken $T$-$T$ bonds in monoclinic $Tb_5Si_2Ge_2$ are much smaller than the rest of the Tb moments.[27] Such magnetic frustration weakens ferromagnetism upon cooling as evidenced by the

ZFC-FC irreversibility (Fig. 3) and the lower saturation magnetization (inset of Fig. 2). The presence of the FM-M phase indicates a decoupled magnetostructural transition,[27] leading to a reduced MCE in $Tb_5(Si_xGe_{1-x})_4$ compared to $Gd_5(Si_xGe_{1-x})_4$. Adding Si eliminates the FM-M phase from the ground state, as confirmed by a fully restored FM O(I) phase in $Tb_5(Si_{0.7}Ge_{0.3})_4$. For this composition, the ZFC-FC irreversibility nearly disappears and a higher ordering temperature is observed due to strengthened FM exchange interactions.

Our previous work shows that the magnetostructural properties of $R_5(Si_xGe_{1-x})_4$ can be modified by Si doping and/or applied pressure in a similar fashion. For $Gd_5(Si_xGe_{1-x})_4$, both Si doping and applied pressure trigger an AFM O(II) $\rightarrow$ FM O(I) transition involving the reforming of inter-slab bonding, along with a linear enhancement of $T_C$.[12,13] For $Tb_5(Si_xGe_{1-x})_4$, XRD (Fig. 1) and SQUID (Fig. 3) results show that Si doping causes a canted AFM O(II) to FM O(I) transformation. It is, therefore, reasonable to expect that pressure would result in the same transition, based on the analogy with the Gd-based compounds. This is indeed seen in Fig. 4. For $Tb_5(Si_{0.4}Ge_{0.6})_4$, the canted AFM O(II) $\rightarrow$ FM O(I) transition can also be realized by pressure, which confirms the existence of the Si doping–pressure correspondence in $Tb_5(Si_xGe_{1-x})_4$. This finding is in agreement with previous pressure-dependent results reported for $Tb_5(Si_{0.5}Ge_{0.5})_4$,[27] and extends the Si doping–pressure correspondence to higher pressures. Note that once the canted AFM O(II) to FM O(I) transition is complete, further increases in pressure stabilize FM ordering by increasing the transition temperature alone, as can be seen in the data at 4 and 7 GPa [Fig. 4(a)].

Although the canted AFM $\rightarrow$ FM transition can be achieved by either Si doping or pressure, they occur with different electronic modifications. This is highlighted in Fig. 5, where the XANES white line peak intensity decreases with increasing pressure, but not with Si doping. Furthermore, the line shapes of Tb $L_3$-edge XMCD are similar for low and high Si doping, but they are markedly different for ambient- and high-pressure data at the position where the quadrupolar contribution dominates. For $Tb_5(Si_xGe_{1-x})_4$, pressure causes a detectable increase in the XMCD quadrupolar feature, perhaps due to a lifting of $4f$ states across the Fermi level accompanied by changes in $5d$ occupation. It is important to note that the XMCD of $Tb_5(Si_{0.4}Ge_{0.6})_4$ at $P = 7$ GPa is expected to be close to that of $Tb_5(Si_{0.7}Ge_{0.3})_4$ at ambient pressure, because both of them reach a fully saturated FM O(I) ground state. However, the dipolar XMCD signal at $P = 7$ GPa is smaller than that of $Tb_5(Si_{0.7}Ge_{0.3})_4$ by $\sim$12%. Considering the concomitant increase in quadrupolar XMCD signal the result suggests that there is likely a $4f$-$5d$ charge transfer taking place while the material undergoes the transition under pressure (but to a much lesser extent upon Si doping). The enhanced XMCD signal in the quadrupolar channel indicates that such newly formed empty $4f$ states are spin polarized. The decrease of the XANES intensity in the dipolar channel with pressure could be due to a related decrease in the empty Tb $5d$ states in the vicinity of the Fermi level, also responsible for the broadening of the XMCD signal. Such putative $4f$-$5d$ hybridization could facilitate FM interactions

and lead to increasing magnetic ordering temperatures. Since the transition temperature keeps increasing from 4 to 7 GPa even though the $4f$-$5d$ hybridization does not, the strength of indirect FM exchange in $Tb_5(Si_xGe_{1-x})_4$ is not only regulated by this assumed $4f$-$5d$ hybridization. Additional contributions to the enhancement of the ordering temperature for $P > 4$ GPa may come from increased $5d$–Si (Ge) $p$ hybridization, as was observed in $Gd_5(Si_xGe_{1-x})_4$.[12] Density functional theoretical calculations in the local density $+ U$ approximation (LDA $+ U$) are needed in order to address the exact nature of the pressure-induced changes in electronic structure.

On the other hand, the $4f$-$5d$ orbital hybridization is minor in $Gd_5(Si_xGe_{1-x})_4$ where XMCD broadening and enhancement of quadrupolar features, either in a pressure-induced AFM $\rightarrow$ FM transition[33] or in the further stabilization of the FM state with pressure,[14] are much less visible relative to $Tb_5(Si_xGe_{1-x})_4$. The enhanced stability of the half-filled $4f^7$ configuration of Gd relative to the $4f^8$ configuration of Tb may explain why changes in $4f$ electron occupation and hybridization are observed in the Tb (but not in the Gd) case, even at these moderately low pressures. Furthermore, the sizable single-ion anisotropy of Tb relative to the negligible anisotropy of Gd affects how structural modifications under pressure couple to the $4f$ electronic structure and magnetic ordering.[22] In the case of $Gd_5(Si_xGe_{1-x})_4$ the pressure-induced increase in the FM exchange interactions, as well as the increase in the transition temperature, are mainly facilitated by the change in Gd $5d$–Si (Ge) $p$ hybridization just as with Si doping, rather than by the $4f$-$5d$ hybridization seen in $Tb_5(Si_xGe_{1-x})_4$. This indicates that, although a Si concentration–pressure correspondence is seen in both $Tb_5(Si_xGe_{1-x})_4$ and $Gd_5(Si_xGe_{1-x})_4$, the mechanism by which the strength of FM exchange is regulated differs between the two. The results suggest that in terms of the electronic structure, the Si concentration–pressure correspondence in $Tb_5(Si_xGe_{1-x})_4$ is even more complex than that in $Gd_5(Si_xGe_{1-x})_4$.

The nature of the magnetostructural ground state, in addition to the electronic structure, also determines the response of $Tb_5(Si_xGe_{1-x})_4$ to pressure. As shown in Fig. 6, $Tb_5(Si_{0.4}Ge_{0.6})_4$ yields a discontinuous $dT_t/dP$ as a result of the change in the ground state. The large $dT_t/dP$ for $P < 4$ GPa is due to an effective pressure-induced, first-order canted AFM O(II) $\rightarrow$ FM O(I) transition involving the reforming of the interslab bonds, leading to a sudden stabilization of the FM state. However, for $P > 4$ GPa where the FM O(I) state is fully restored in $Tb_5(Si_{0.4}Ge_{0.6})_4$, the compound exhibits a smaller $dT_c/dP$, comparable to that of $Gd_5(Si_{0.375}Ge_{0.625})_4$, whose ground state is known to be FM O(I). In the latter case, pressure acts to stabilize the FM O(I) state, slowly increasing $T_t$.

## V. CONCLUSION

We have measured, using SQUID, XRD, and XMCD probes, the magnetostructural properties of $Tb_5(Si_xGe_{1-x})_4$ ($x = 0.4$, 0.485, 0.625, and 0.7) in response to Si doping and applied pressure. It is found that a full FM O(I) ground state is only observed for $x \geqslant 0.7$, while the other three samples display either canted AFM O(II) ($x = 0.4$) or mixed FM [M + O(I)]

($x = 0.485$ and $0.625$) phases. The $Tb_5(Si_xGe_{1-x})_4$ family responds to Si doping and pressure in a similar way, resulting in the FM O(I) ground state when the canted AFM O(II) phase of $x = 0.4$ is doped with Si or subjected to pressure. This is similar to its Gd counterpart.[14,15] However, a remarkable electronic modification involving Tb $4f$ and $5d$ states accompanies the canted AFM $\rightarrow$ FM transition in $Tb_5(Si_xGe_{1-x})_4$ with pressure but not with Si doping. Such involvement of $4f$ states does not appear to occur in $Gd_5(Si_xGe_{1-x})_4$. The larger sensitivity of $4f$ states to pressure in the Tb system lies in its modified electronic band structure relative to that of the Gd system. In addition, the $dT_t/dP$ is strongly dependent on the material's magnetostructural ground state, another factor that determines the $Tb_5(Si_xGe_{1-x})_4$ response to pressure.

*Corresponding author: yctseng21@mail.nctu.edu.tw; yuanchieh.tseng@gmail.com

[1] Z. B. Guo, J. R. Zhang, H. Huang, W. P. Ding, and Y. W. Du, Appl. Phys. Lett. **70**, 904 (1997).

[2] V. K. Pecharsky and K. A. Gschneidner Jr., J. Alloys. Compd. **260**, 98 (1997).

[3] V. K. Pecharsky and K. A. Gschneidner Jr., Adv. Mater. **13**, 683 (2000).

[4] E. Warburg, Ann. Phys. Chem. **13**, 141 (1881).

[5] L. Morellon, C. Magen, P. A. Algarabel, M. R. Ibarra, and C. Ritter, Appl. Phys. Lett. **79**, 1318 (2001).

[6] V. V. Ivtchenko, V. K. Pecharsky, and K. A. Gschneidner Jr., Adv. Cryo. Eng. **46A**, 405 (2000).

[7] C. Magen, L. Morellon, P. A. Algarabel, M. R. Ibarra, C. Ritter, A. O. Pecharsky, K. A. Gschneidner, and V. K. Pecharsky, Phys. Rev. B **70**, 224429 (2004).

[8] C. Ritter, C. Magen, L. Morellon, P. A. Algarabel, M. R. Ibarra, A. M. Pereira, J. P. Araujo, and J. B. Sousa, Phys. Rev. B **80**, 104427 (2009).

[9] C. Ritter, L. Morellon, P. A. Algarabel, C. Magen, and M. R. Ibarra, Phys. Rev. B **65**, 094405 (2002).

[10] P. Schobinger-Papamantellos, J. Phys. Chem. Solids **39**, 197 (1978).

[11] L. Morellon, C. Ritter, C. Magen, P. A. Algarabel, and M. R. Ibarra, Phys. Rev. B **68**, 024417 (2003).

[12] D. Haskel, Y. B. Lee, B. N. Harmon, Z. Islam, J. C. Lang, G. Srajer, Ya. Mudryk, K. A. Gschneidner Jr., and V. K. Pecharsky, Phys. Rev. Lett. **98**, 247205 (2007).

[13] D. Haskel, Y. C. Tseng, J. C. Lang, and S. Sinogeikin, Rev. Sci. Instrum. **78**, 083904 (2007).

[14] Y. C. Tseng, D. Haskel, J. C. Lang, S. Sinogeikin, Ya. Mudryk, V. K. Pecharsky, and K. A. Gschneidner Jr., Phys. Rev. B **76**, 014411 (2007).

[15] Y. C. Tseng, D. Haskel, N. M. Souza-Neto, Ya. Mudryk, V. K. Pecharsky, and K. A. Gschneidner Jr., Phys. Rev. B **78**, 214433 (2008).

[16] M. Zou, V. K. Pecharsky, K. A. Gschneidner Jr., Ya. Mudryk, D. L. Schlagel, and T. A. Lograsso, Phys. Rev. B **80**, 174411 (2009).

[17] A. P. Hammersley, S. O. Svensson, M. Hanfland, A. N. Fitch, and D. Hausermann, High Press. Res. **14**, 235 (1996).

[18] L. B. McCusker, R. B. Von Dreele, D. E. Cox, D. Louër, and P. Scardi, J. Appl. Crystallogr. **32**, 36 (1999).

[19] A.P. Holm, V. K. Pecharsky, K. A. Gschneidner Jr., R. Rink, and M. N. Jirmanus, Rev. Sci. Instrum. **75**, 1081 (2004).

[20] V. K. Pecharsky, A. P. Holm, K. A. Gschneidner Jr., and R. Rink, Phys. Rev. Lett. **91**, 197204 (2003).

[21] E. M. Levin, K. A. Gschneidner Jr., T. A. Lograsso, D. L. Schlagel, and V. K. Pecharsky, Phys. Rev. B **69**, 144428 (2004).

[22] M. Zou, Ya. Mudryk, V. K. Pecharsky, K. A. Gschneidner Jr., D. L. Schlagel, and T. A. Lograsso, Phys. Rev. B **75**, 024418 (2007).

[23] Paolo Carra, B. N. Harmon, B. T. Thole, M. Altarelli, and G. A. Sawatzky, Phys. Rev. Lett. **66**, 2495 (1991).

[24] N. M. Souza-Neto, D. Haskel, Y. C. Tseng and Gerard Lapertot, Phys. Rev. Lett. **102**, 057206 (2009).

[25] A. Rogalev and J. Goulon, in *X-ray and Inner-shell Processes*, edited by D. S. Gemmell, S. H. Southworth, R. W. Dunford, E. P. Kanter, and L. Young, AIP Conf. Proc. No. 506 (AIP, Melville, NY, 2000), p. 336.

[26] Y. C. Tseng, D. Haskel, J. C. Lang, Ya. Mudryk, V. K. Pecharsky, and K. A. Gschneidner Jr., J. Appl. Phys. **103**, 07B301 (2008).

[27] L. Morellon, Z. Arnold, C. Magen, C. Ritter, O. Prokhnenko, Y. Skorokhod, P. A. Algarabel, M. R. Ibarra, and J. Kamarad, Phys. Rev. Lett. **93**, 137201 (2004).

[28] V. Hardy, S. Majumdar, S. J. Crowe, M. R. Lees, D. Mck. Paul, L. Hervé, A. Maignan, S. Hébert, C. Martin, C. Yaicle, M. Hervieu, and B. Raveau, Phys. Rev. B **69**, 020407(R) (2004).

[29] E. M. Levin, K. A. Gschneidner Jr., and V. K. Pecharsky, Phys. Rev. B **65**, 214427 (2002).

[30] V. K. Pecharsky, A. O. Pecharsky, Y. Mozharivskyj, K. A. Gschneidner Jr., and G. J. Miller, Phys. Rev. Lett. **91**, 207205 (2003).

[31] Y. Mozharivskyj, A. O. Pecharsky, V. K. Pecharsky, G. J. Miller, and K. A. Gschneidner Jr., Phys. Rev. B **69**, 144102 (2004).

[32] J. M. Cadogan, D. H. Ryan, Z. Altounian, X. Liu, and I. P. Swainson, J. Appl. Phys. **95**, 7076 (2004).

[33] D. Haskel, Y.C. Tseng, N. M. Souza Neto, J. C. Lang, S. Sinogeikin, Ya. Mudryk, K. A. Gschneidner Jr., and V. Pecharsky, High Press. Res. **28**, 185 (2008).